Journal of Materials Chemistry A

Accepted Manuscript

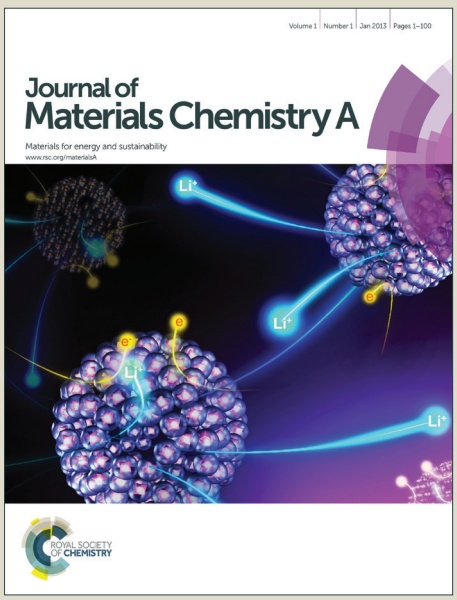

ROYAL SOCIETY OF CHEMISTRY

www.rsc.org/materialsA

Journal of Materials Chemistry A RSC Publishing

ARTICLE

Dynamic Hydrophobic Hindrance Effect of Zeolite@Zeolitic Imidazolate Framework Composites for CO_2 Capture in the Presence of Water

Fei Gao,[a] Yankai Li,[a] Zijun Bian,[a] Jun Hu*[a] and Honglai Liu*[b]

Cite this: DOI: 10.1039/x0xx00000x

Received 00th January 2012,
Accepted 00th January 2012

DOI: 10.1039/x0xx00000x

www.rsc.org/

For the real industrial process of CO_2 capture, it is still a great challenge for adsorbents to exhibit excellent CO_2 adsorption capacity in the presence of water. By combining a pre-seeding process and a two-step temperature controlling crystallization, zeolitic imidazolate framework (ZIF-8) shell is introduced on the commercial zeolite adsorbent (5A) core to produce a series of 5A@ZIF-8 composites with an enhanced surface hydrophobicity. Each 5A@ZIF-8 composite exhibits a dynamic hydrophobic hindrance effect for the separation CO_2 from the simulated humid flue gas (15% CO_2 and 90% humidity at 298 K). Among them, the CO_2 adsorption capacity and the CO_2/H_2O selectivity of 5A@ZIF-8(I) can be as high as 2.67 mmol g^{-1} and 6.61 at the optimized adsorption time of 10 min. More importantly, over 10 adsorption-desorption cycles, there is almost no degradation of adsorption performance. Therefore, the novel strategy of utilizing the dynamic hydrophobic hindrance effect through a core-shell structure would be a good solution for improving the CO_2 separation performance in practical applications.

Introduction

Carbon dioxide capture and storage (CCS), an effective strategy to reduce the carbon dioxide emissions from the flue gas of power plants and auto exhausts, has attracted considerable research efforts.[1] Adsorption technique has been approved as one of the most promising options for CCS because of the low capital investment cost, low energy consumption and easiness to achieve automatic operation.[2-3] It is well known that the selection of excellent adsorbents is a key factor in adsorption process. There have been many potential adsorbent candidates for CO_2 capture, such as zeolites,[4-5] activated carbons,[6] and metal-organic frameworks (MOFs).[7-9] Among them, commercially available zeolites, such as 5A and 13X, have received tremendous industrial attention since they have high CO_2 adsorption capacity at normal pressure and are less expensive. However, in many humid cases, such as the separation of CO_2 from the flue gas or the biogas, most of the sorbents would lose their good CO_2 adsorption performance because of the better affinity for H_2O molecules.[10-12] Webley group studied the CO_2 capture on zeolite 13X from humid flue gas containing 3.4 % (vol.) of water vapour at 30 °C by vacuum swing adsorption, and the result indicated a relatively low purity (59 % CO_2) and recovery (68 %).[13] At present, dehumidification is a necessary process before the CO_2 capture, which significantly increases the total energy consumption and investment cost.[14] Therefore, developing novel adsorbents with a high CO_2 adsorption capacity even under humid conditions would be extremely meaningful for real industrial applications.

So far, two strategies have been utilized to effectively overcome this humidity challenge. Firstly, the chemical adsorption is used to make H_2O molecule participate in the adsorption reaction, such as various amine modified porous materials.[15-16] Very recently, Yaghi's group reported well designed materials of amyloid fibers[17], amine functionalized metal organic framework (MOF) material, IRMOF-74-III[18] as effective adsorbents for CO_2 capture under humid conditions. Secondly, well designed hydrophobic adsorbents are used to resist H_2O molecule adsorption.[19] However, all these materials should be elegantly designed and carefully fabricated, which would be far away from the real industrial utilization. Considering the outstanding CO_2 capture ability of commercial zeolites under dry conditions, we propose a novel strategy that a dynamic hydrophobic hindrance effect is utilized in which a hydrophobic porous shell would be introduced on cheap zeolite adsorbents to prevent the prior adsorption of H_2O molecules. Consequently, with the optimized operation conditions, such as the adsorption time, the zeolite adsorbents would still exhibit an excellent CO_2 adsorption capacity even in the presence of water.

For hydrophobic porous materials, zeolite imidazolate frameworks (ZIFs) [20-21], a type of hybrid inorganic-organic material, has received tremendous attention. Among various ZIFs, ZIF-8, with a large pore of 11.6 Å connected through small apertures of 3.4 Å, has been well studied.[22-25] Because of the flexible pore apertures and relatively hydrophobic surface,

it has shown promising performances including significantly enhanced gas permeability and selective adsorption capacity towards less polar molecules. Recently, ZIF-8 composite materials with hierarchical structures have attracted significant research interests in prospect of water vapor separation.[26-29] Simultaneously, the efforts dedicated to the synthesis of various composite structures, such as the core-shell structure[29-32], make progresses in the fabrication of new types of zeolite and ZIF composites.

Herein, we design a convenient core-shell structure adsorbent, in which the commercial zeolite adsorbent acts as the core to maintain the high CO_2 adsorption capacity, and a hydrophobic porous material as the shell to dynamically hinder the entrance of H_2O molecules into the core. Typically, the core-shell 5A@ZIF-8 composites were selected and fabricated to verify our proposal. Through a pre-seeding process and a two-step temperature controlling crystallization synthesis approach (Scheme 1) a ZIF-8 shell was grown up on the surface of zeolite 5A microparticles. Moreover, we established a convenient method through the joint of the thermogravimetric analysis and the mass spectrometry (TG-MS) to quantitatively demonstrate the performance of CO_2 dynamic separation from the simulated humid flue gas. To the best of our knowledge, the utilization of the dynamic hydrophobic hindrance effect of the core-shell structure under practical humid conditions has not ever been reported.

Experimental

Materials

5A zeolite powder was purchased from Shanghai Jiuzhou Chemicals Co. Ltd., Zinc nitrate hexahydrate ($Zn(NO_3)_2{\cdot}6H_2O$, > 98 %) was purchased from Sinopharm Chemical Reagents Co., Ltd. 2-methylimidazole (> 99 %) was purchased from Sigma-Aldrich. Methanol (99.99 %) was purchased from Shanghai Titanchem Co., Ltd. All chemicals were used without further purification.

Synthesis of 5A@ZIF-8 composites

As illustrated in Scheme 1, the synthesis combines a pre-seeding process and a two-step temperature controlling crystallization for further growth of crystals, in which, the former is very important to form a homogeneous and completely covered ZIF-8 shell, while the latter is used to control the size and distribution of ZIF-8 crystals. Typically, 5A zeolite powder was first activated by heating at 300 °C for 5 h before use. 0.372 g of $Zn(NO_3)_2{\cdot}6H_2O$ was dissolved in 25 mL methanol (denoted as solution A) and 0.308 g of 2-methylimidazole was dissolved in 75 mL methanol (denoted as solution B). Then 0.5 g of activated 5A zeolite powder was dispersed in a mix solution consist of 1 mL solution A and 3 mL solution B with ultrasonication for 1 min. After centrifugation, the precursor-enriched 5A powder was separated and placed on a glass plate which was immediately moved into a 100 °C oven for fast solvent evaporation and crystal seeds formation. Afterwards, a two-step temperature controlling crystallization was used for further growth of ZIF-8 crystals. The pre-seeded 5A powder was redispersed in the ZIF-8 precursor solution consist of 24 mL solution A and 72 mL solution B, followed by stirring for 2 h at -15 °C and another 2 h at room temperature. The resultant product was separated and collected with filtration, washing for three times by methanol and subsequently dried at 100 °C under vacuum overnight. This process was carried out once for 5A@ZIF-8(I), twice for 5A@ZIF-8(II) and three times for 5A@ZIF-8(III).

Moreover, pristine ZIF-8 sample[33], 5A@ZIF-8 materials without either of the pre-seeding process or the two-step temperature controlling crystallization were also synthesized for comparisons.

Characterizations

Field-emission scanning electron microscope (FESEM) images were taken by using a Nova NanoSEM 450. Powder X-ray diffraction (PXRD) patterns were recorded on a D/Max2550 VB/PC spectrometer using Cu Kα radiation (40 kV and 200 mA). Fourier transform infrared (FTIR) spectra of the samples were recorded at room temperature on a Thermo Scientific Nicolet iS10. Nitrogen adsorption measurements were conducted at 77.4 K on a Micrometrics ASAP 2020 sorptionmeter. The total surface area was determined by the Brunauer-Emmett-Teller (BET) model, the microporous area was determined by the *t*-plot method, and the mesoporous area was calculated by the total BET surface area minus the microporous area. The size distribution of the mesopores was determined by Barrett-Joyner-Halenda (BJH) model, while the size distribution of the micropores was determined by Horvath–Kawazoe (HK) model. Thermogravimetric analysis (TG) measurements were performed on a Netzsch STA 449 F3 Jupiter. Mass Spectrometry (MS) measurements were conducted on a Netzsch QMS 403 D Aëolos. Water contact angle (CA) experiments were performed on a JC2000Y contact angle equipment of Powereach.

Gases adsorption measurements

CO_2 and N_2 adsorption capacities of the samples were determined by a Micrometrics ASAP 2020 at 25 °C and all samples were degassed for 12 h at 150 °C under vacuum before the measurement. The ideal selectivity of CO_2 to N_2 was determined by the slope ratio of the initial segments of CO_2 adsorption isotherm at lower pressure to that of N_2 adsorption isotherm.

To examine the CO_2 adsorption performance of the obtained 5A@ZIF-8 composites in the presence of water, we proposed a practicable quantitative method through the joint TG-MS. The samples were first degassed in pure N_2 stream with a flow rate of 20 ml/min at 250 °C for 5 h in the oven of the thermogravimetric analyzer. After cooling down to 25 °C, the samples were exposed to a simulated flue gas, in which 90% relative humidity was introduced into the gas mixture of CO_2 and N_2 with the fixed ratio of $15CO_2$:$85N_2$ (vol/vol). The

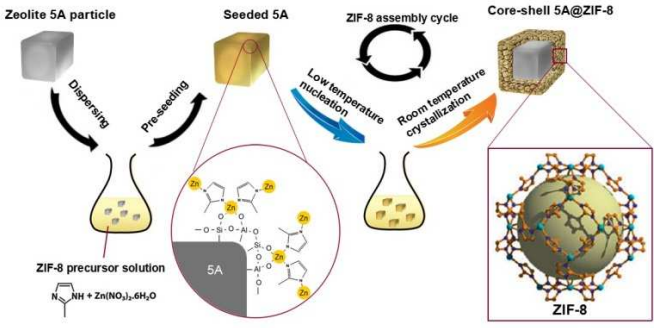

Scheme 1 Schematic illustration of the synthesis approach of the 5A@ZIF-8.

adsorption was taken place under the humid CO_2/N_2 mixture feed stream. The flow rate of the whole feed steam was 20 ml/min. Then a purge desorption for 60 min, followed by a thermal desorption up to 250 °C with a heating rate of 5 °C/min were carried out under pure N_2 with the flow rate of 20 ml/min. The signals of the mass loss of the samples as well as the mass spectrometry of H_2O (mass/charge ratio = 18) were recorded simultaneously during the desorption process. For calculation of the adsorption capacities of H_2O and CO_2, a calibration experiment was conducted, in which 5A zeolite was exposed to humid N_2 feed stream (90% relative humidity but without CO_2) for the adsorption, while the following thermal desorption process and other conditions remained the same.

Results and discussion

The morphology and structure of the obtained 5A@ZIF-8 composites with different ZIF-8 assembly cycles are shown in Fig. 1a-i and their properties are summarized in Table 1. A good coverage of ZIF-8 shell on the surface of 5A particles can be observed after only one ZIF-8 assembly cycle (5A@ZIF-8(I), Fig. 1a-c). The average size of the ZIF-8 nanocrystals is about 100 nm (the inset of Fig. 1b), and the very thin shell of 5A@ZIF-8(I) composite (Fig. 1c) indicates only one or two layers of ZIF-8 nanocrystals covered on the surface of 5A. The highly compact ZIF-8 shell is attributable to the successful nucleation of ZIF-8 occurring on the surface of 5A particles (Fig. S1a, Electronic Supplementary Information, ESI) through the interaction between the surface silanol groups of 5A and Zn^{2+} cations during the pre-seeding process (Scheme 1). While one-pot synthesis without the pre-seeding process would lead to the self-formation of the ZIF-8 crystals in the bulk solution and poor coverage of ZIF-8 on the 5A core (Fig. S1c and d). Moreover, a two-step temperature controlling crystallization process, including a low temperature at -15 °C followed by a room temperature crystallization, ensures the continuous growth of the ZIF-8 shell on the surface of 5A particles. As a contrast, the room temperature crystallization without the temperature controlling would produce an uneven ZIF-8 shell with obvious defects on the surface of 5A particles (Fig. S1b). The thickness of the ZIF-8 shell can be controlled by altering the assembly cycle (Scheme 1). After the second (5A@ZIF-8(II), Fig. 1d-f) and the third assembly cycle (5A@ZIF-8(III), Fig. 1g-i), the ZIF-8 shell becomes significantly thicker and denser.

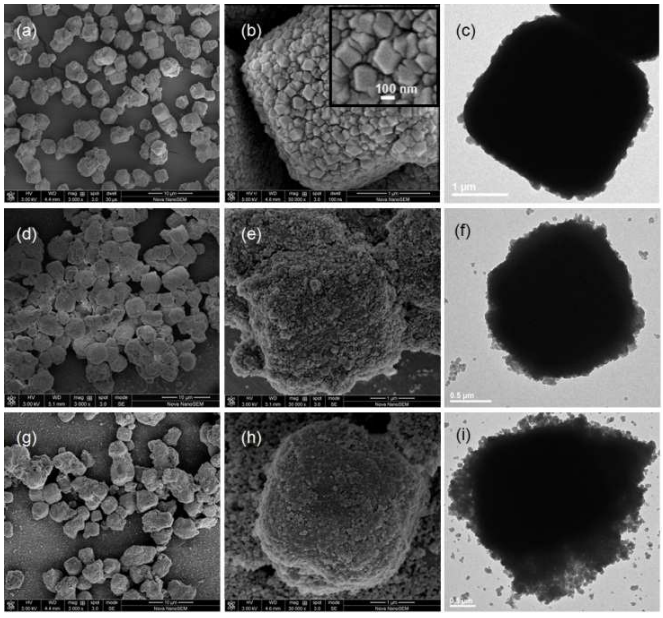

Fig. 1 SEM and TEM images of 5A@ZIF-8 core-shell particles after one ZIF-8 assembly cycle (a, b and c), two cycles (d, e and f) and three cycles (g, h and i).

The PXRD patterns (Fig. 2a) and the FTIR spectra (Fig. 2b) further demonstrate the formation of 5A@ZIF-8 composites. Compared with the reference samples of pristine 5A and ZIF-8, the PXRD patterns of the 5A@ZIF-8 composites show the presence of the characteristic peaks of both 5A and ZIF-8 samples. Meanwhile, with the increase of the ZIF-8 assembly cycle, the intensities of the characteristic peaks of ZIF-8 grow stronger regularly while the characteristics of 5A decrease. Similar changes are also observed in the FTIR spectra. Furthermore, the weight percentages of ZIF-8 in 5A@ZIF-8 composites can be approximately determined by the mass loss on the TG curves (Fig. S2) measured under N_2 atmosphere. It is estimated that the contents of ZIF-8 in 5A@ZIF-8(I), 5A@ZIF-8(II) and 5A@ZIF-8(III) composites are about 21.6, 32.4 and 47.6 wt.%, respectively. The porosities (Table 1) of 5A@ZIF-8 composites, determined by the N_2 adsorption isotherms at 77 K, show that the BET surface area (total pore volume) are in the increasing sequence of 379 (0.23), 467 (0.28) and 645 (0.40)

Table 1 Surface area, total pore volume, thermodynamic CO_2 uptake, CO_2/N_2 selectivity, dynamic CO_2 uptake and CO_2/H_2O selectivity for each sample.

Sample	ZIF content [wt. %]	A_{BET} [$m^2\ g^{-1}$] [a]	V_{total} [$cm^3\ g^{-1}$][b]	CO_2 uptake [mmol g^{-1}][c]	N_2 uptake [mmol g^{-1}] [c]	CO_2/N_2 selectivity[d]	CO_2 uptake-wet [mmol g^{-1}][e]	CO_2/H_2O selectivity[e]
ZIF-8	100	880	0.46	0.67	0.47	1.91	0.32	0.28
5A	0	334	0.18	3.68	0.31	58.5	0.73	0.07
5A@ZIF-8(I)	21.6	379	0.23	2.97	0.31	30.6	2.74	0.76
5A@ZIF-8(II)	32.4	467	0.28	2.61	0.35	22.2	2.55	0.96
5A@ZIF-8(III)	47.6	645	0.40	2.06	0.39	14.8	1.57	0.60

[a] Calculated by BET method. [b] Calculated at the point of P/P_0=0.99. [c] At 1 bar and 298 K. [d] Calculated from the initial segment of pure component isotherms. [e] Calculated from dynamic adsorption experiments after exposed to the simulated flue gas for 2 h.

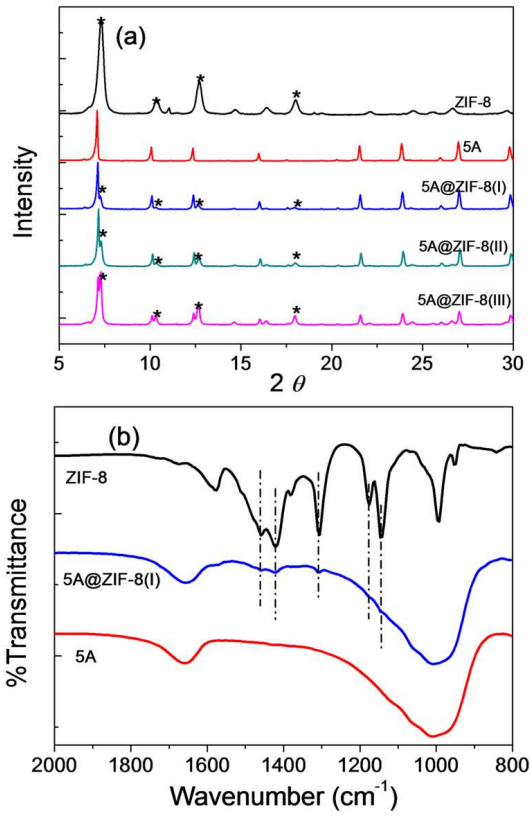

Fig. 2 (a) PXRD patterns and (b) FTIR spectra of 5A, ZIF-8 and 5A@ZIF-8 composites, respectively.

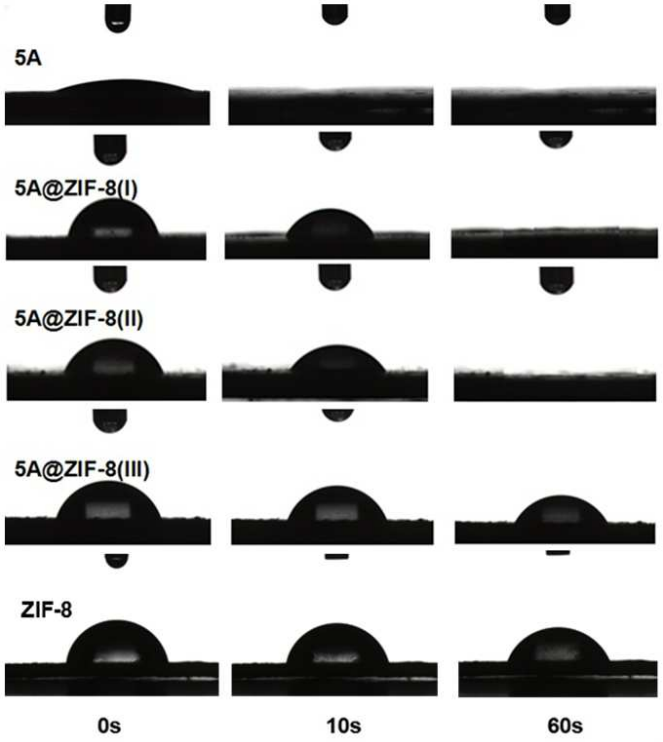

Fig. 3 Comparisons of water contact angles on 5A, 5A@ZIF-8(I), 5A@ZIF-8(II), 5A@ZIF-8(III) and ZIF-8 with different durations.

m^2g^{-1} (cm^3g^{-1}) for 5A@ZIF-8(I), 5A@ZIF-8(II) and 5A@ZIF-8(III), respectively. The corresponding pore size distribution curves (Fig. S3) show the existence of dual-porosity, i.e., 0.46 nm micropores attributed to the intrinsic porosities of 5A and ZIF-8, and 3.1 nm mesopores caused by the intercrystalline voids in ZIF-8 shell. Without any significant macropores detected, it further reveals the well-compacted coverage of ZIF-8 shell.

The improvements of the surface hydrophobicity of 5A@ZIF-8 composites with different ZIF-8 assembly cycles were investigated by CA measurement. Each sample powder was pressed into a plate before the measurement. As shown in Fig. 3, when a water droplet was brought in contact with the surface of pristine 5A plate, it was quickly absorbed in a few seconds, and the CA was nearly zero, revealing its superior hydrophilicity. While for 5A@ZIF-8 composites, all CAs were measured to be around 80° when water droplets just contacted the sample plates, attributed to the good coverage architecture of ZIF-8 shell, which were in accordance with their SEM image. It is worthy to mention that after the first ZIF-8 assembly cycle, 5A@ZIF-8(I) composite already significantly improved the hydrophobicity. However, despite the hydrophobic character of ZIF-8, water could slowly infiltrate into the composites through the intercrystalline voids in ZIF-8 shell. After 1 min, water droplet totally infiltrated into 5A@ZIF-8(I) composite plate. As expected, with more ZIF-8 assembly cycles, more complete coverage with the relatively hydrophobic shell would more efficiently hinder the entrance of water molecules into the inner 5A core. As a result, the water

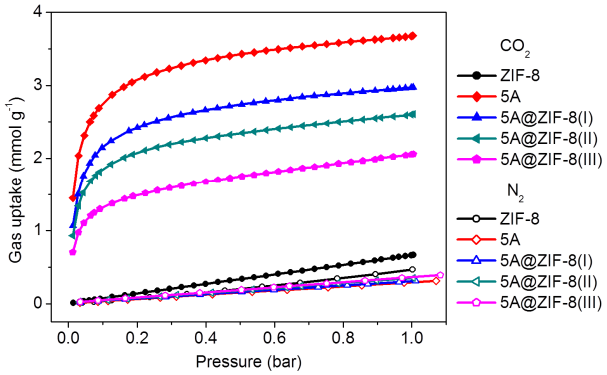

Fig. 4 CO_2 and N_2 adsorption isotherms of each sample collected at 298 K.

droplet could maintain more than 1 min on the surface of 5A@ZIF-8(III) plate, which can be comparable with the pristine ZIF-8.

CO_2 adsorption capacity and the CO_2/N_2 selectivity are two most important parameters for evaluating the feasibility of adsorbents. Pure CO_2 and N_2 adsorption isotherms at 298 K are collected on 5A and 5A@ZIF-8 composites samples (Fig. 4), respectively. 5A@ZIF-8(I) composite shows a good CO_2 adsorption capacity of 2.97 mmol g^{-1} at 1 bar, a little lower than that of pristine 5A zeolite (3.67 mmol g^{-1}), because of the lower CO_2 adsorption capacity of pristine ZIF-8 under the same measurement conditions (0.67 mmol g^{-1}). Consequently, as summarized in Table 1, with more ZIF-8 assembly cycles, the

CO_2 adsorption capacities of 5A@ZIF-8(II and III) show a significant decrease. Comparatively, the N_2 adsorption capacities are much lower than that of CO_2. Since the CO_2 content in the real flue gas is usually lower than 15 %, we can use the initial segment of the adsorption isotherms (Fig. S4) to estimate the ideal selectivity of CO_2/N_2, which are in a descending order from 58.5 for 5A zeolite, 30.6, 22.2, and 14.8 for 5A@ZIF-8(I), 5A@ZIF-8(II) and 5A@ZIF-8(III) composite, respectively. The CO_2/N_2 selectivity of the composite material decreases with more ZIF-8 content, and is lower than that of pure 5A. This is because ZIF-8 has a better affinity for less polar molecules (N_2).

For the real CO_2 capture from the post-combustion flue gas, the influence of water could not be ignored. Although some well-designed experimental devices and column breakthrough experiments were used to evaluate the ability of CO_2 dynamic adsorption in the presence of water, most of them are reported as qualitative or half-quantitative comparisons.[17-19,34-35] In this contribution, we developed a dynamic adsorption strategy based on a convenient quantitative determining method through the joint of TG-MS. Since the dynamic CO_2 and N_2 uptakes cannot be directly determined by the MS measurement (detailed explanation in the below of Fig. S5), we used the ideal CO_2/N_2 selectivity instead of the real CO_2/N_2 selectivity to evaluate the CO_2 adsorption performance of adsorbents. As we have discussed, the adsorption selectivity of CO_2 or H_2O towards N_2 of all 5A@ZIF-8 composites is so high that the amount of N_2 adsorbed could be negligible, therefore, the weight increase (or loss) during the adsorption (or desorption) process is only attributed to the adsorption (or desorption) of CO_2 and H_2O. Meanwhile, a MS was used to monitor the amount of desorbed H_2O in the effluent during the desorption process. Because the MS peak area of H_2O is proportional to the amount of H_2O adsorbed in the sample, we can compare the MS peak areas of H_2O to estimate the amount of H_2O adsorbed on samples. To obtain the proportionality coefficient R_{H2O} (the ratio of mass/area), we established a calibration curve (Fig. S5) by using the dynamic adsorption strategy in which only the humid N_2 feed stream (90% relative humidity but without CO_2) was used. When pristine 5A sample was exposed in the humid N_2 for a series of time, such as 5, 10, 20, 30 and 60 min, different amounts of H_2O were adsorbed in the sample. Since we supposed the mass loss during the desorption stage is only attributed to the removal of adsorbed H_2O, plotting the mass loss of each case against the corresponding area of peak in its H_2O MS curve, the linear fitting curve gives the value of the slope (R_{H2O}) as 2.432×10^5. On this basis, the H_2O uptakes from the simulated flue gas for any samples can be calculated by multiplying the peak area in its corresponding H_2O MS curve by R_{H2O}, and then, the CO_2 uptakes can be estimated by subtracting the calculated amount of H_2O from the total mass increase in the TG curve during the adsorption process.

Fig. 5a shows the typical dynamic adsorption breakthrough and desorption curves determined by TG when the sample was exposed to the simulated flue gas containing 15 % (v/v) of CO_2 in N_2 with 90% relative humidity, followed by a thermal desorption under the purge of pure N_2, meanwhile, MS was used to monitor the amount of H_2O desorbed in the effluent during the desorption process. The H_2O and CO_2 uptakes of all samples after adsorbing for 2 h were calculated and summarized in Table S1. All 5A@ZIF-8 composites show a significantly improved CO_2 capacity and CO_2/ H_2O selectivity under the humid condition compared with the pristine 5A zeolite, indicating the successful designing methodology of introducing a porous hydrophobic shell on a cheap commercially available adsorbent.

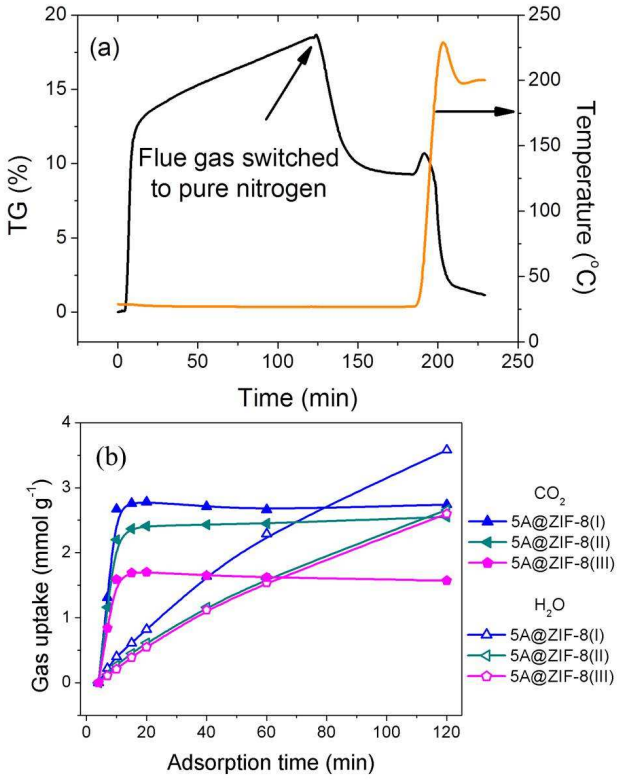

Fig. 5 (a) Dynamic adsorption breakthrough and desorption curve of 5A@ZIF-8(I) from the simulated flue gas in the presence of water; (b) Dynamic uptakes of H_2O and CO_2 after adsorption for different times.

Since the dynamic adsorption breakthrough curve (Fig. 5a) still shows a steadily increased trend even after adsorbing for 2 h, the adsorptions of CO_2 and H_2O are far from equilibrium. To explicate the variation rules of competitive adsorptions between CO_2 and H_2O during the adsorption process and hence to optimize the adsorption conditions, the dynamic adsorption was further investigated by exposing each 5A@ZIF-8 composite to the simulated flue gas for a series of periods, such as 7, 10, 15, 20, 40, 60, and 120 min. The details of CO_2 and H_2O uptakes at each point were analyzed and summarized in Table S2-3 and Fig. 5b. As shown in Fig. 5b, during the initial adsorption process before 10 min, the CO_2 uptake of each sample increases steeply and then quickly approaches the saturation with only very little H_2O adsorbed. After that, the CO_2 uptake keeps nearly unchanged; while the H_2O uptake undergoes an almost linear increase. The CO_2 uptakes at 10 min of all samples show almost twice of those at 7 min, and the saturated CO_2 uptakes are in a descending order of 5A@ZIF-8(I) (2.7 mmol g^{-1}) > 5A@ZIF-8(II) (2.4 mmol g^{-1}) > 5A@ZIF-8(III) (1.6 mmol g^{-1}), which is in accordance with the results of CO_2 adsorption isotherms. Because the ZIF-8 component has a relatively poor CO_2 adsorption capacity, more ZIF-8 assembly cycles would improve the water resistance and degrade the CO_2 uptake as well. On the other hand, the slopes of the initial stage of water adsorption curves for the three samples are about 0.060, 0.047 and 0.033, respectively, with a descending order, indicating the

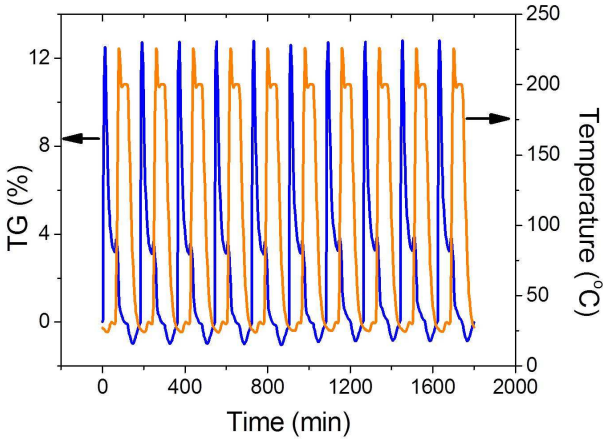

Fig. 6 10-cycle stability of adsorption and desorption on 5A@ZIF-8(I) from the simulated flue gas with the adsorption time of 10 min.

enhanced water hindrance with thicker ZIF-8 shell. Therefore, the CO_2/H_2O selectivities at the inflection point of 10 min for 5A@ZIF-8 composites are as high as 6.61, 8.15 and 7.57, respectively; after that, the CO_2/H_2O selectivity of all samples show a significant descent. These phenomena indicate that the relatively hydrophobic ZIF-8 shell can effectively hinder the entrance of water molecules but allow the free diffusion of CO_2 molecules into the inner 5A core, maintaining the overall good affinity to CO_2 in the initial adsorption stage. However, H_2O molecules can still gradually penetrate into the sample with the adsorption time prolonged, resulting in a continuous increase of H_2O uptake. Accordingly, there is an inflection point at about 10 min in the breakthrough curve (Fig. 5a), before that, the fast increase of the weight is mainly attributed to the CO_2 uptake; whereas, the slow increase after the inflection point is just caused by the H_2O uptake. Therefore, for real industrial application, the 5A@ZIF-8 composites can effectively capture CO_2 in the presence of water vapor in an optimized operation time. Although the water uptakes continue increasing after 10 min, the CO_2 uptakes do not change a lot. So 10 min would be the optimized operation time for CO_2 adsorption from the simulated flue gas in the presence of water on 5A@ZIF-8 composites. Considering the CO_2 adsorption capacity, the CO_2 adsorption selectivity to N_2 and H_2O, as well as the synthesis convenience, 5A@ZIF-8(I) composite would be a preferable choice for further use of the dynamic removal of CO_2 from the humid flue gas.

Moreover, the recycle stability is also a very important parameter for the real CO_2 capture. When the adsorption time was fixed at the optimized time of 10 min, 10 circular adsorption-desorption performance on 5A@ZIF-8(I) from the same simulated flue gas (Fig. 6) reveals its high separation stability that there is almost no change can be observed in the adsorption-desorption cycle curves. It is worthy to mention that the CO_2 uptake and the CO_2/H_2O selectivity maintain as high as 2.61 mmol g^{-1} and 6.03 after ten adsorption-desorption cycles. Also, the well-maintained PXRD pattern of 5A@ZIF-8(I) after 10 cycles (Fig. S8) further confirms its structure stability. Besides, 5A@ZIF-8 composites exhibit superior thermal stability with the decomposition temperature as high as 550 °C in N_2 atmosphere (Fig. S2).

Conclusions

In summary, we reported a new type of porous core–shell 5A@ZIF-8 composites. By combining a pre-seeding process and a two-step temperature controlling crystallization process, ZIF-8 shell was successfully assembled on the surface of 5A zeolite core, which significantly improved the surface hydrophobic property, and hence hindered the entrance of water molecules into the inner 5A core. Based on our quantitative determining method, the dynamic CO_2 uptake and the CO_2/H_2O selectivity from the humid flue gas were quantitatively evaluated by the joint of TG-MS device. With only one assembly cycle, the core-shell 5A@ZIF-8(I) composite already showed a significantly enhanced selective CO_2 adsorption performance. The CO_2 uptake and the CO_2/H_2O selectivity could maintain as high as 2.61 mmol g^{-1} and 6.03 after 10 adsorption-desorption cycles with the optimized adsorption time of 10 min. We expect this novel strategy of utilizing the dynamic hydrophobic hindrance effect by introducing a porous hydrophobic shell on a cheap commercially available adsorbent to form a core-shell structure, as well as the proposed quantitative determining method through the joint of TG-MS device could provide good solutions in the future real industrial CO_2 capture processes.

Acknowledgements

We sincerely thank Prof. Dongyuan Zhao for his helpful comments and suggestions.

Financial supports for this work are provided by the National Basic Research Program of China (2013CB733501), the National Natural Science Foundation of China (No. 91334203, 21176066), the 111 Project of China (No.B08021), the Fundamental Research Funds for the Central Universities of China and the project of FP7-PEOPLE-2013-IRSES (PIRSES-GA-2013-612230).

Notes and references

[a] *Key Laboratory for Advanced Materials, East China University of Science and Technology, 130 Meilong Road, Shanghai 200237, China. E-mail: junhu@ecust.edu.cn; Fax: 86-21-64252195; Tel: 86-21-64252195*

[b] *State Key Laboratory of Chemical Engineering and Department of Chemistry, East China University of Science and Technology, 130 Meilong Road, Shanghai 200237, China. E-mail: hlliu@ecust.edu.cn; Fax: 86-21-64252921; Tel: 86-21-64252921*

† Electronic Supplementary Information (ESI) available: [SEM images, TG curves, N_2 sorption isotherms, CO_2/N_2 ideal selectivities and MS curves of H_2O for the corresponding samples]. See DOI: 10.1039/b000000x/

1 C. Song, *Catal. Today*., 2006, **115**, 2-32.

2 D. Aaron, C. Tsouris, *Sep. Sci. Technol.*, 2005, **40**, 321-348.

3 A. Chaffee, G. P. Knowles, Z. Liang, J. Zhang, P. Xiao, P. A. Webley, *Int. J. Greenh. Gas Con.*, 2007, **1**, 11-18.

4 S. K. Wirawan, D. Creaser, *Microporous Mesoporous Mater.*, 2006, **91**, 196-205.

5 F. Su, C. Lu, S.-C. Kuo, W. Zeng, *Energy Fuels* 2010, **24**, 1441-1448.

6 K. T. Chue, J. N. Kim, Y. J. Yoo, S. H. Cho, R. T. Yang, *Ind. Eng. Chem. Res.*, 1995, **34**, 591-598.

7 A. R. Millward, O. M. Yaghi, *J. Am. Chem. Soc.*, 2005, **127**, 17998-17999.

8 J. J. Gassensmith, H. Furukawa, R. A. Smaldone, R. S. Forgan, Y. Y. Botros, O. M. Yaghi, J. F. Stoddart, *J. Am. Chem. Soc.*, 2011, **133**, 15312-15315.

9 K. Sumida, D. L. Rogow, J. A. Mason, T. M. McDonald, E. D. Bloch, Z. R. Herm, T. H. Bae, J. R. Long, *Chem. Rev.*, 2012, **112**, 724-781.

10 S. S. Kaye, A. Dailly, O. M. Yaghi, J. R. Long, *J. Am. Chem. Soc.*, 2007, **129**, 14176-14177.

11 J. J. Low, A. I. Benin, P. Jakubczak, J. F. Abrahamian, S. A. Faheem, R. R. Willis, *J. Am. Chem. Soc.*, 2009, **131**, 15834-15842.

12 P. Nugent, Y. Belmabkhout, S. D. Burd, A. J. Cairns, R. Luebke, K. Forrest, T. Pham, S. Ma, B. Space, L. Wojtas, M. Eddaoudi, M. J. Zaworotko, *Nature*, 2013, **495**, 80-84.

13 G. Li, P. Xiao, P. Webley, J. Zhang, R. Singh and M. Marshall, *Adsorption*, 2008, **14**, 415-422.

14 G. Li, P. Xiao, P. A. Webley, J. Zhang, R. Singh, *Energy Procedia*, 2009, **1**, 1123-1130.

15 S. Choi, J. H. Drese and C. W. Jones, *ChemSusChem*, 2009, **2**, 796-854.

16 A. Samanta, A. Zhao, G. K. H. Shimizu, P. Sarkar and R. Gupta, *Ind. Eng. Chem. Res.*, 2012, **51**, 1438-1463.

17 D. Li, H. Furukawa, H. Deng, C. Liu, O. M. Yaghi, D. S. Eisenberg, *PNAS*, 2014, **111**, 191-196.

18 A. M. Fracaroli, H. Furukawa, M. Suzuki, M. Dodd, S. Okajima, F. Gándara, J. A. Reimer, O. M. Yaghi, *J. Am. Chem. Soc.*, 2014, **136**, 8863-8866.

19 N. T. Nguyen, H. Furukawa, F. Gandara, H. T. Nguyen, K. E. Cordova and O. M. Yaghi, *Angew. Chem. Int. Ed.*, 2014, **53**, 10645-10648.

20 X. C. Huang, Y. Y. Lin, J. P. Zhang and X. M. Chen, *Angew. Chem. Int. Ed.*, 2006, **45**, 1557-1559.

21 J. P. Zhang, Y. B. Zhang, J. B. Lin and X. M. Chen, *Chem. Rev.*, 2012, **112**, 1001-1033.

22 R. Kumar, K. Jayaramulu, T. K. Maji, C. N. Rao, *Chem. Commun.*, 2013, **49**, 4947-4949.

23 R. Li, X. Ren, X. Feng, X. Li, C. Hu, B. Wang, *Chem. Commun.*, 2014, **50**, 6894-6897.

24 L. Dumée, L. He, M. Hill, B. Zhu, M. Duke, J. Schütz, F. She, H. Wang, S. Gray, P. Hodgson, L. Kong, *J. Mater. Chem.*, 2013, **1**, 9208-9214.

25 M. Zahmakiran, *Dalton Trans.*, 2012, **41**, 12690-12696.

26 Y. Y. Fu, C. X. Yang, X. P. Yan, *Chem. Eur. J.*, 2013, **19**, 13484-13491.

27 Y.-C. Sue, J.-W. Wu, S.-E. Chung, C.-H. Kang, K.-L. Tung, K. C. W. Wu, F.-K. Shieh, *ACS Appl. Mater. Interfaces*, 2014, **6**, 5192-5198.

28 T. Zhang, X. Zhang, X. Yan, L. Lin, H. Liu, J. Qiu, K. L. Yeung, *Catal. Today.*, 2014, **236**, 41-48.

29 S. Sorribas, B. Zornoza, C. Tellez, J. Coronas, *Chem. Commun.*, 2012, **48**, 9388-9390.

30 Y. Liu, W. Zhang, S. Li, C. Cui, J. Wu, H. Chen and F. Huo, *Chem. Mater.,* 2014, **26**, 1119-1125.

31 M. Zhao, K. Deng, L. He, Y. Liu, G. Li, H. Zhao and Z. Tang, *J. Am. Chem. Soc.*, 2014, **136**, 1738-1741.

32 C.-F. Zhang, L.-G. Qiu, F. Ke, Y.-J. Zhu, Y.-P. Yuan, G. Xu and X. Jiang, *J. Mater. Chem. A*, 2013, **1**, 14329-14334.

33 A. J. Amali, J.-K. Sun and Q. Xu, *Chem. Commun.*, 2014, **50**, 1519-1522.

34 P. Nugent, Y. Belmabkhout, S. D. Burd, A. J. Cairns, R. Luebke, K. Forrest, T. Pham, S. Ma, B. Space, L. Wojtas, M. Eddaoudi and M. J. Zaworotko, *Nature*, 2013, **495**, 80-84.

35 O. Shekhah, Y. Belmabkhout, Z. Chen, V. Guillerm, A. Cairns, K. Adil and M. Eddaoudi, *Nat. Commun.*, 2014, **5**, 4228.

Graphical abstract